Ultrathin films of L1$_0$-MnAl on GaAs (001): A hard magnetic MnAl layer onto a soft Mn-Ga-As-Al interface

C. Navío, M. Villanueva, E. Céspedes, F. Mompeán, M. García-Hernández, J. Camarero, and A. Bollero

View Online   Export Citation   CrossMark

ARTICLES YOU MAY BE INTERESTED IN

Saturation magnetization and crystalline anisotropy calculations for MnAl permanent magnet
Journal of Applied Physics **107**, 09A731 (2010); https://doi.org/10.1063/1.3337640

Fabrication of L1$_0$-MnAl perpendicularly magnetized thin films for perpendicular magnetic tunnel junctions
Journal of Applied Physics **111**, 07A324 (2012); https://doi.org/10.1063/1.3676428

MnBi thin films for high temperature permanent magnet applications
AIP Advances **9**, 035325 (2019); https://doi.org/10.1063/1.5080004

Ultrathin films of L1$_0$-MnAl on GaAs (001): A hard magnetic MnAl layer onto a soft Mn-Ga-As-Al interface

C. Navío,[1] M. Villanueva,[1] E. Céspedes,[1] F. Mompeán,[2]
M. García-Hernández,[2] J. Camarero,[1,3] and A. Bollero[1]

[1]*Division of Permanent Magnets and Applications, IMDEA Nanoscience, Madrid 28049, Spain*
[2]*Instituto de Ciencia de Materiales de Madrid, ICMM-CSIC, Madrid 28049, Spain*
[3]*Condensed Matter Physics Department, Autónoma University of Madrid (UAM), Madrid 28049, Spain*

Ferromagnetic MnAl (L1$_0$-MnAl phase) ultrathin films with thickness varying from 1 to 5 nm have been epitaxially grown on a GaAs (001) substrate. A coercivity above 8 kOe has been obtained with no need of a buffer layer by tuning the sample preparation and the growth parameters. Surface and interface analysis carried out by *in situ* characterization techniques (x-ray photoelectron spectroscopy and low energy electron diffraction), available in the molecular beam epitaxy chamber, has shown the formation of a ferromagnetic interface consisting of Mn-Ga-As-Al, which contribution competes with the MnAl alloyed film. The appearance of this interface provides important information to understand the growth mechanism of MnAl-based films reported in the literature. © *2018 Author(s). All article content, except where otherwise noted, is licensed under a Creative Commons Attribution (CC BY) license (http://creativecommons.org/licenses/by/4.0/).* https://doi.org/10.1063/1.5050852

Thin films with perpendicular magnetic anisotropy are attracting a lot of interest in spintronic devices, in particular in STT-MRAM (Spin-Transfer-Torque Magnetic Random Access Memory) and p-MTJs (perpendicular magnetic tunnel junctions).[1,2] In order to obtain high thermal stability and low switching current density in p-MTJ, the ferromagnetic layers that conform the MTJ must have large perpendicular magnetic anisotropy and low saturation magnetization. Among others, ordered binary manganese-based alloys with equiatomic ratio are proposed as good candidates for this objective. In particular, one of the alloys, the ferromagnetic L1$_0$-MnAl (or τ-MnAl), is in a metastable phase so that the conditions for obtaining good L1$_0$-MnAl films are strongly restricted.[2–8] In addition, the L1$_0$-MnAl is a rare-earth free material that it has been proposed for certain applications as rare earth free permanent magnets,[6,9–14] due to their well known high magnetic anisotropy constants.[1,15] In spite of the instability of the L1$_0$-MnAl phase, once the films are grown, the L1$_0$-MnAl phase becomes stable at room temperature and the growth on different semiconductors enhances the potential applications of the obtained heterostructure on the fields of spintronics, ultrahigh-density recording media, and nonvolatile magnetoresistive random access memory.[1,16–18]

In this study, ultrathin films of MnAl have been grown on GaAs (001) by MBE (Molecular Beam Epitaxy) with thickness varying from 1 to 5 nm. XPS (X-ray Photoelectron Spectroscopy) and LEED (Low Energy Electron Diffraction) were performed *in situ* in order to characterize the chemical states and the arrangement of the surface atoms. Magnetic and structural characterization was performed *ex situ* by SQUID (Semiconducting Quantum Interference Device magnetometry) and XRD (X-Ray Diffraction). XPS and X-ray diffraction reflectivity results were used to accurately determine the thickness of the films, which allowed for determination of magnetization values from the SQUID measurements. XPS measurements were performed under Ultra-High Vacuum conditions (UHV, with a base pressure of 7×10^{-10} mbar), using a monochromatic Al Kα line as an exciting photon source for core level analysis (hν = 1486.7 eV). The emitted photoelectrons were collected in a hemispherical energy analyzer (SPHERA-U7, pass energy set to 20 eV for the XPS measurements to have a resolution of 0.6 eV). The crystal structure of the films was examined by X-ray diffraction (XRD) in θ-2θ geometry using Cu K$_\alpha$ radiation (Bruker D8 Advance). Magnetic properties were
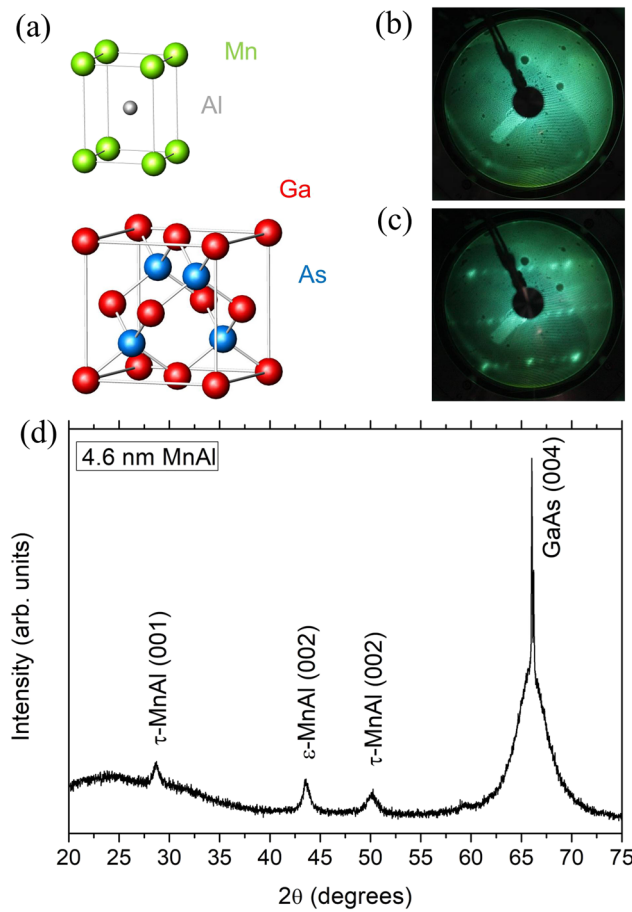
FIG. 1. (a) Schematic ideal structure of $L1_0$-MnAl (τ-MnAl) on GaAs substrate with its corresponding LEED patterns taken at 40 eV of (b) 2 nm of MnAl grown on GaAs (001) at 100 °C plus 400 °C of postgrowth annealing and (c) clean GaAs (001) substrate. (d) X-ray diffraction pattern for a layer of 4.6 nm of MnAl grown on GaAs (001) at 250 °C.

measured by SQUID magnetometry (Quantum Design MPMS) up to 50 kOe with a magnetic field applied both parallel and perpendicular to the film at 300 and 5 K. The properties of the $L1_0$-MnAl phase are very sensitive to the growth conditions[5,8,9] and, due to the difficulties on obtaining this ferromagnetic phase, a substrate of GaAs (001) is going to be used to induce the epitaxial growth. The lattice parameter of GaAs (001) is 0.565 nm, and the $L1_0$-MnAl has a tetragonally distorted structure with a = 0.277 nm and c = 0.354 nm [see Fig. 1(a)]. In order to obtain the perpendicular magnetization with respect to the surface (of interest for magnetic storage applications), the MnAl layer has to be grown as it is shown in Fig. 1(a), which means that the lattice mismatch will be 1.9%, compatible with a good epitaxial growth (<9%). An ideal structure of the system is shown in Fig. 1(a), where it is represented by the wurtzite structure of the GaAs and the tetragonal $L1_0$-MnAl on it. Ferromagnetism of $L1_0$-MnAl structure is related to the increase in the Mn-Mn atomic distance (compared to the Mn metal one), to 2.96 Å or more, due to the Al presence.[20] The choice of the GaAs substrate is not only due to epitaxial reasons: GaAs is a very well known and studied semiconductor, and there are many studies that point toward the advantages of the growth of heterostructure ferromagnetic-semiconductor in spintronics.[16,18,21]

The MnAl films were grown by molecular beam epitaxy (MBE) by alternating monolayers of Mn and Al on GaAs (001). The GaAs substrates were prepared *in situ* with typical ultrahigh vacuum cleaning procedures to remove the native oxide: cycles of Ar^+ sputtering plus annealing at 550 °C, obtaining afterwards a 2 × 4 surface reconstruction as a starting point [see the LEED pattern in Fig. 1(c)]. The MnAl films were grown keeping the substrate at different temperatures (from 100 to 250 °C), applying a postgrowth thermal treatment at 400 °C when the growth was performed at

100 °C. To prevent from ambient oxidation, a capping layer of Ta with a nominal thickness of 5 nm was deposited before the sample was withdrawn from the UHV system. In all the cases, the MnAl film showed a LEED pattern as the one shown in Fig. 1(b), with the expected 1×1 surface reconstruction. The results revealed the importance of the growth temperature for the final properties of the magnetic film: it was necessary to keep the substrate above room temperature during the growth in order to have ferromagnetic response. It is important to notice that no buffer layer was needed for the growth of the $L1_0$-MnAl phase.

The structure of the as-deposited $L1_0$-MnAl film was measured by *ex situ* X-Ray Diffraction (XRD). Figure 1(d) shows the diffraction pattern of a 4.6 nm thick film of $L1_0$-MnAl grown on GaAs (001) at 250 °C, with the two main reflections of the $L1_0$-MnAl phase in register with the substrate orientation, evidencing c-axis $L1_0$-MnAl along the normal direction as it was expected for the epitaxial growth. This result is completely correlated with the magnetic properties shown in Fig. 2, where there is a strong magnetic anisotropy with the easy axis laying perpendicular to the sample surface (out-of-plane). The additional peak in the diffraction pattern centered at 43.6° can
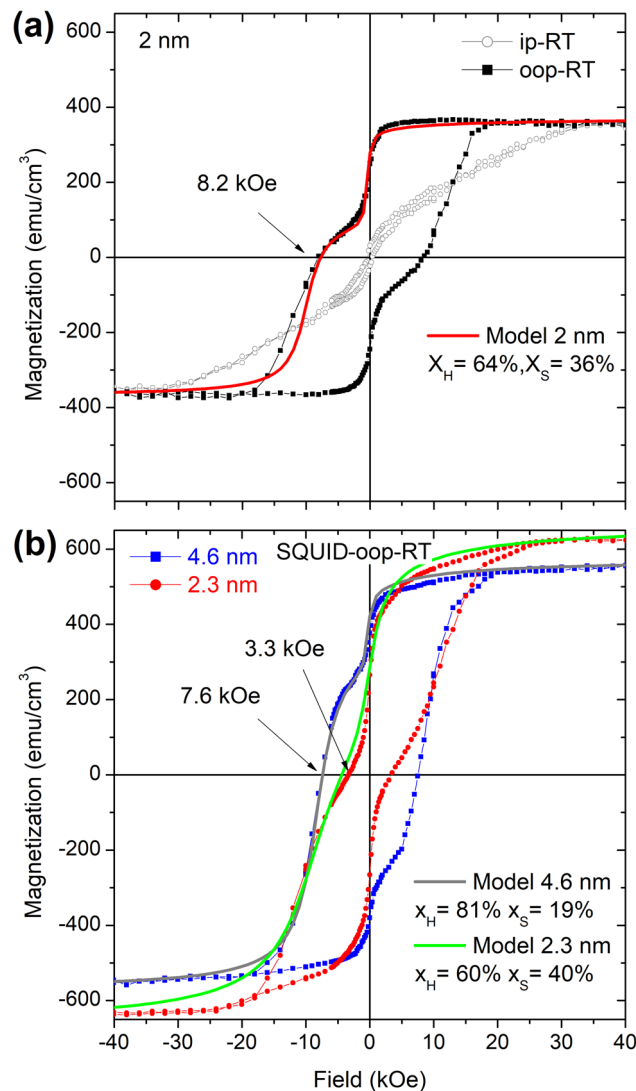
FIG. 2. SQUID measurements of (a) 2 nm of MnAl grown on GaAs (001) at 100 °C with a postgrowth annealing process of 400 °C, with the out of plane (oop) component in full black squares and the in plane (ip) one in open white circles. On panel (b), the oop SQUID measurements for a 2.3 and 4.6 nm of MnAl grown on GaAs (001) at 250 °C. Modeling of the hysteresis demagnetization curves with different hard and soft phase ratios (x_H and x_S, respectively) is shown as continuous lines.

be assigned to the nonmagnetic hexagonal-closed-packed ε-MnAl (002) phase,[21,22] which is a stable phase of Mn-Al. If the annealing temperature of the sample increases up to 400-450 °C, the L1$_0$-MnAl reflections disappear, while the ε-MnAl (002) is maintained (not shown). Diffraction peaks from the ε (002) structure were also observed by Nie *et al.*[5] for annealing temperatures above 250 °C in epitaxial MnAl films grown on GaAs (001) by MBE using different buffer layers. The (002) reflection of the GaAs substrate is almost totally absent (only a small structure around 2θ = 31.6° is visible in the noise level), a fact that can be attributed to the introduction of defects during the cleaning process: the native oxide was removed with the Ar+ sputtering. Indeed, the GaAs (004) peak is not very intense and the full with at half maximum is too large for a good single crystal.[5] The average grain size on the perpendicular direction to the surface can be obtained from the FWHM (Full Width at Half Maximum) of the diffractions peaks using the Scherrer equation. In this case, it can be compared to the film thickness, with a resulting value of 5 nm, which is in good agreement with the estimation performed by XPS (4.6 nm). Note that a large crystalline ε-MnAl contribution (about the L1$_0$-MnAl one) is evidenced by XRD, which can have an important effect on the net magnetic moment reduction.

The room temperature magnetic properties of the L1$_0$-MnAl films were determined by using SQUID magnetometry. Figure 2(a) shows the magnetic response of the sample in the perpendicular direction of the film surface (out of plane contribution, oop) and the in plane (ip) one for a MnAl film with a thickness of 2 nm on GaAs (001), grown at 100 °C with a post-growth annealing at 400 °C. A strong perpendicular magnetic anisotropy is evidenced from the determined high anisotropy field of about 30 kOe [Fig. 2(a)]. This result is consistent with the diffraction patterns [Fig. 1(d)], where only the (hkl) Bragg peaks in register with the substrate orientation appear, the *001* family. Accordingly, only the oop component of the hysteresis loop is going to be shown for the following samples under study. The hysteresis loop in Fig. 2(a) has a coercivity of 8.2 kOe and a saturation magnetization of 370 emu/cm^3. This value of coercivity can be considered high for such a low thickness (2 nm) in comparison with values reported in the literature.[5,7,8,11] The saturation magnetization is lower compared with the bulk value (490-600 emu/cm^3),[4,18,23,24] and a clear kink appears in the hysteresis loop. In order to find an explanation to these issues, simulation of the magnetic curves and a set of experiments changing the growth temperature were performed. In Fig. 2(b), the hysteresis loops of two samples grown at 250 °C (no further post-growth treatment applied) show the different magnetic response of the sample by changing the temperature and the thickness (2.3 and 4.6 nm). The 2.3 nm thick film can be compared in thickness with the one of 2 nm prepared under different conditions [Fig. 2(a)]. Based on this, similar magnetic properties might be expected, but a side to side comparison shows that they are indeed significantly different, evidencing the importance of the growth temperature on the final magnetic properties. The coercivity of the sample grown at 250 °C is 3.5 kOe, i.e., less than half the value measured for the sample grown by the two step method (growth at 100 °C followed by a post-growth annealing at 400 °C). On the contrary, the saturation magnetization is much higher on the 2.3 nm thick film: 630 emu/cm^3 compared to 370 emu/cm^3 measured for the 2 nm thick film. In both cases, a kink in the hysteresis loop is observed indicative of a softer magnetic phase reversing at an applied magnetic field lower than that of the MnAl phase. An increased thickness of the film from 2.3 to 4.6 nm [Fig. 2(b)] shows a diminished contribution of such a softer magnetic phase to the overall magnetic signal of the film.[22,25] Previous studies show a similar kink although with varying magnitude in dependence of the presence of a buffer layer and/or the film thickness,[5,11,16] but the origin of it was in some cases not clear and assigned to film defects or artifacts of the measurement setup.[11]

In order to gauge the relative amounts of hard and soft components (labeled as x$_H$ and x$_S$, respectively) from the hysteresis loops showing a two phase behavior, the experimental curves were simulated as a sum of two individual loops. An empirical equation that describes the magnetization response of a ferromagnetic sample comprised of n independently switching magnetic phases was used.[12] The simulated curves (continuous lines) reproduce most of the experimental features, well in agreement with the coexistence of both hard (τ-MnAl) and soft (interface phase). Obtained x$_H$ and x$_S$ ratios are, with decreasing hard phase content, x$_H$ = 81% and x$_S$ = 19% for 4.6 nm, x$_H$ = 64% and x$_S$ = 36% for 2 nm, and x$_H$ = 60%, x$_S$ = 40% for 2.3 nm sample. The soft phase thickness can be calculated from these values, obtaining 0.7-0.9 nm of the soft phase in all cases, expected at the

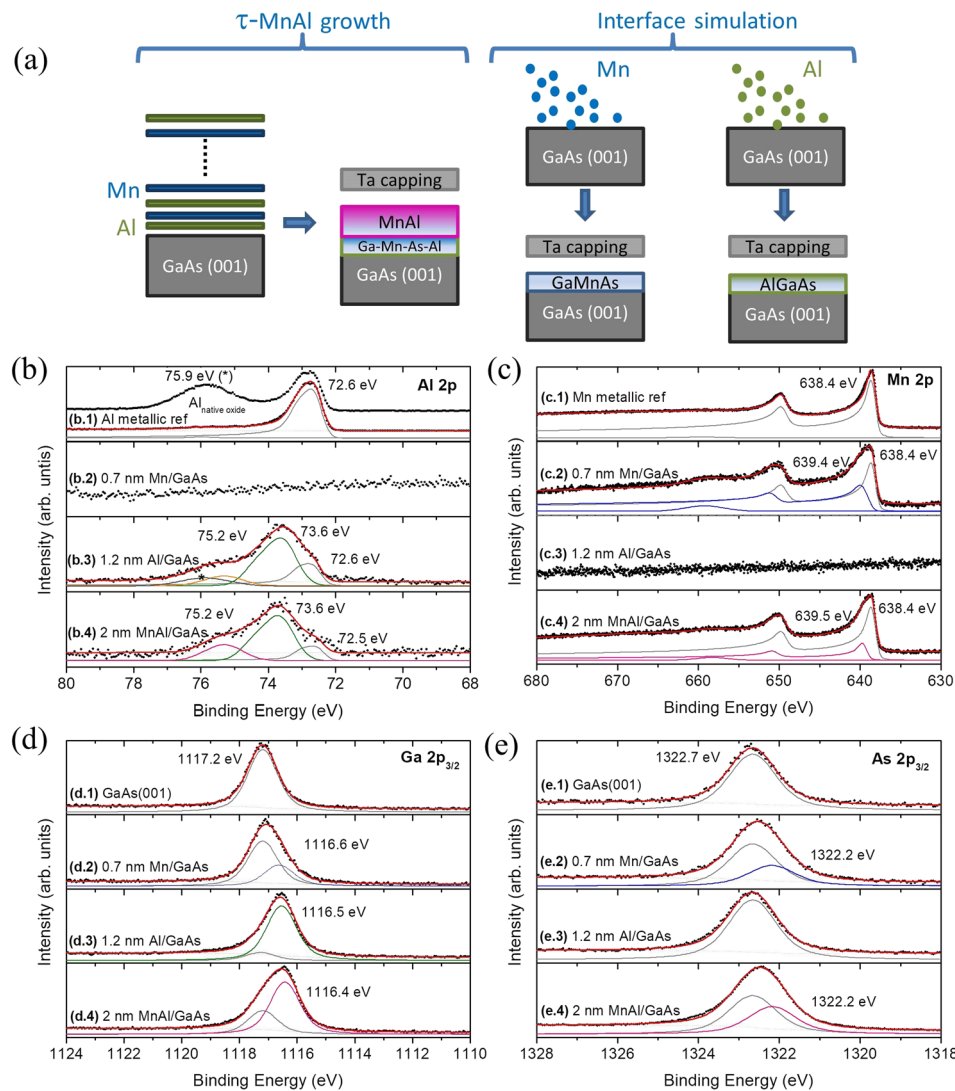FIG. 3. Experimental schema (a) and XPS core levels for representative references and of 2 nm of MnAl grown on GaAs (001) at 100 °C with a postgrowth annealing process of 400 °C, (b) Al 2p, (c) Mn 2p, (d) Ga $2p_{3/2}$, and (e) As $2p_{3/2}$. The black filled circles represent the experimental data, and all the data are normalized to the maximum intensity to better observe the binding energy changes.

substrate-MnAl interface. τ-MnAl phase, and related to the hard magnetic component, is shown to coexist with ε-MnAl by XRD, being its presence associated with a reduced net magnetic moment.

The MBE chamber where the samples were grown was connected to an XPS, so it was possible to measure *in situ* the chemical states of the $L1_0$-MnAl films. Due to the low thickness of the grown layers, the substrate and the interface could be studied as well. Figure 3 summarizes the experimental studied systems [Fig. 3(a)] and the changes in the core levels of the substrate and the representative peaks of the samples: Al $2p_{3/2}$, Mn $2p_{3/2}$, Ga 2p, and As 2p corresponding to panels in Figs. 3(b)–3(e). The Fermi level was taken as a binding energy reference because in the case of the substrate (a semiconductor), before cleaning for the removal of the native oxide, the typical carbon peak coming for the atmospheric exposure made the sample conductive. In these conditions, all the core levels were also measured (not shown) and the oxide component was well discriminated from the clean GaAs, placing the Ga $2p_{3/2}$ and the As $2p_{3/2}$ in 1117.2 eV and 1322.7 eV, respectively. These two spectra are shown in Figs. 3(d.1) and 3(e.1), in combination with that of the clean GaAs substrate (before the growth) as a reference.

After the growth of $L1_0$-MnAl, it could be expected in a first approximation one component for the Al peak and its corresponding on the Mn core level. In the case of Al [Fig. 3(b.4)], there are three components clearly visible on the 2 nm MnAl sample: the one at lower binding energy can be assigned to an excess of metallic aluminum, i.e., metallic Al used as an evaporation material [see reference sample in Fig. 3(b.1) panel], but it is not straightforward to determine the other two. Taking into account the position of the aluminum oxide on the reference sample, none of the unnamed components can be assigned to oxidation in Al. Moreover, in most of the experiments, there were no traces of oxygen detected with XPS, so it is necessary to study in detail the rest of the elements involved on the film. For the Mn 2p [Fig. 3(d.4)], one chemical state is observed, but its binding energy is the same as the Mn metallic reference, i.e., metallic Mn material used as the evaporation material [Fig. 3(c.1)], and it is too broad for being only metallic Mn, so the peak fit in the spectrum [Fig. 3(d.4)] was performed using two components: the first one with all the features of metallic Mn but the intensity (position, width, and asymmetry fixed) and a second component to fill the necessary part of the core level. This procedure gave the information that there is a part of the Mn that it is not bonded with Al, so in the sample, there is $L1_0$-MnAl and an excess of metallic Mn and Al. The second component obtained on the Mn is placed at 639.5 eV with the peak fit, i.e., 1.1 eV at higher binding energy with respect to the reference that could be assigned as the Mn of the $L1_0$-MnAl phase. There is, however, an unidentified third component on the Al peak which makes it necessary to analyze the substrate.

The panels (d) and (e) of Fig. 3 represent the most intense core levels for the substrate: Ga $2p_{3/2}$ and As $2p_{3/2}$. Before the $L1_0$-MnAl growth, both Ga and As show a unique clean component [see Figs. 3(d.1) and 3(e.1), respectively], but after the growth, there is a new component at lower binding energies: 0.8 and 0.5 eV from the Ga and As references, respectively. In order to understand this complex system and the elements that form the interface between the $L1_0$-MnAl film and the GaAs (001) substrate, two types of experiments were performed to simulate the interface compound. On the first experiment, a very thin film of Mn (0.7 nm) was deposited on the GaAs (001) substrate [see Fig. 3(a)], keeping the rest of experimental conditions identical as those used for the $L1_0$-MnAl phase. In this case, the Mn 2p core level [see Fig. 3(c.2)] shows two components: a metallic one and other different than the second component in Fig. 3(c.4): the binding energy is centered at 639.4 eV, the full width at half maximum (FWHM) is 1.6 eV [1.2 eV for the sample in Fig. 3(c.4)], and the satellite peaks at 659.2 eV, while in the $L1_0$-MnAl phase, it is in 658.3 eV. Even the asymmetry parameter and the doublet distance are different: the asymmetry for Fig. 3(c.2) is 0.58 while 0.43 for Fig. 3(c.4) and the metallic Mn reference. The doublet is separated by 11.2 eV for Figs. 3(c.4) and 3(c.1) while 11.3 eV for Fig. 3(c.2). Now that the formation of a Mn-based compound, different to $L1_0$-MnAl, is evident, an analysis of the variations found on the substrate is needed to discern the compositional nature of the interface. Again, both Ga and As show the appearance of a lower binding energy component, quite similar in the case of As compared with the $L1_0$-MnAl [see Figs. 3(e.2) and 3(e.4)] but different in the case of Ga [Fig. 3(d.2) with Fig. 3(d.4)], not only in the position but on the relative amount with the Ga reference component. All of these variations point toward the formation of a Ga-Mn-As compound, where the Mn component must be overlapped/hidden in the case of $L1_0$-MnAl. Note also that the metallic Mn component evidenced by XPS might have a detrimental effect on the net sample magnetization regarding if leading to an antiferromagnetic long-range order. As well, it is important to take into account that ε-MnAl contribution, shown by XRD, might be indistinguishable from the $L1_0$-MnAl one by XPS.

The second experiment, now aimed to simulate the interface of $L1_0$-MnAl and GaAs, consisted on evaporating a very thin film of Al on GaAs, in the same conditions that the Mn experiment was performed before. Figure 3(b.3) shows the Al 2p peak with the same three components that the $L1_0$-MnAl has [Fig. 3(b.4)] but with the relevant difference that in this experiment, there is no Mn on the sample, i.e., implying that all these bonds are with the substrate. In the case of Ga [Fig. 3(d.3)], there is a second component similar to the one formed in $L1_0$-MnAl, but in this experiments, there is no variation on the As core level. These results point toward the formation of a GaAl layer, which is the main contribution in the Al 2p peak or to Ga-Al-As with the As compound signal overlapped with the substrate one, i.e., making impossible its discrimination. This result is very useful for the identification in the Al 2p of $L1_0$-MnAl, where the interface compound is located at this binding energy, 73.6 eV,
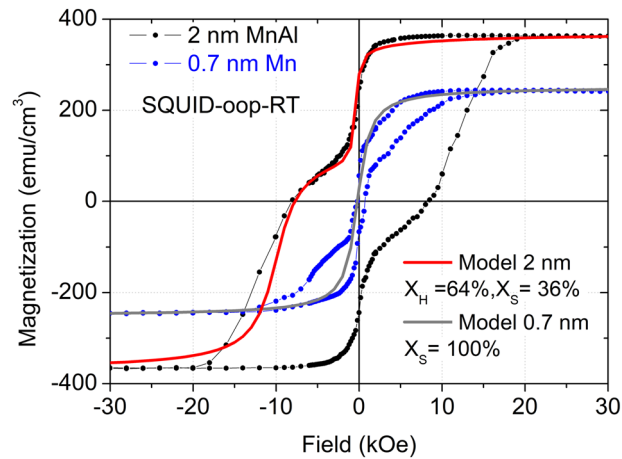
FIG. 4. SQUID measurements of 2 nm of MnAl grown on GaAs (001) at 100 °C with a postgrowth annealing process of 400 °C (black filled circles) and 0.7 nm of Mn grown at the same conditions on GaAS (001) in blue filled circles. Modeling of the hysteresis demagnetization curves with different hard and soft phase ratios (x_H and x_S, respectively) is shown as continuous lines.

which means that the binding energy position for the Al 2p in $L1_0$-MnAl is centered at 75.2 eV. The same component was also found in the sample with no Mn content [sample Fig. 3(b.3)] that must be bonded with the substrate, but due to the limitations in the resolution, no further component assignment could be achieved.

One of the parameters that can be obtained with XPS is the thickness of the grown film if the film is among the limits of the depth resolution of the technique (6-8 nm). For that purpose, the core level of the substrate is measured before and after the film growth and the attenuation of its signal (area) is proportional to the grown film. Figure 3(d) shows the fits for the clean substrate core level, Ga $2p_{3/2}$, with one component centered in 1117.2 eV. After the growth (in all the samples), another component appears due to the interface compound formation. For the determination of the thickness of the whole layer (MnAl+ interface), only the Ga component relative to the substrate with no reaction (at 1117.2 eV) will be taken into consideration, and for the calculation of the thickness of MnAl, both components of the Ga $2p_{3/2}$ will be used. The sample of 2 nm of MnAl is formed of 1.1 nm of $L1_0$-MnAl and 0.9 nm of interface (Ga-Mn-As-Al), and the sample of 2.3 nm is formed of 1.6 nm of L10-MnAl and 0.7 nm of soft interface. These results are well correlated with the proportions of hard and soft phases simulated in Fig. 2, where the proportion of hard and soft phases were $x_H = 64\%$ and $x_S = 36\%$ for the 2 nm sample and $x_H = 60\%$ and $x_S = 40\%$ for the 2.3 nm sample.

The magnetic contribution of the experimentally simulated interface (blue filled circles) compared to the total signal (black filled circles) is shown in Fig. 4, as well as the modeling of both curves (continuous lines). Note the important kink in the 2 nm sample since the total thickness (2 nm) and the Mn-Al-Ga interface compound (around 0.7 nm) are comparable. The important soft magnetic contribution from the interface is clearly observed, contributing less to the total magnetic response as MnAl increases [seen in Fig. 2(b)]. Note that simulation of the 0.7 nm sample (without Al, with just the interface phase expected) includes only soft phase (100% of x_S), being a good approximation of the experimental curve.

In conclusion, ultrathin (2–4.6 nm) MnAl films showing the ferromagnetic $L1_0$-MnAl phase have been grown, without any buffer layer, and achieving coercivities over 8 kOe. These films show a strong out-of-plane magnetic anisotropy which, in combination with the choice of a semiconductor substrate, may be advantageous for their application in spintronic systems. The *in-situ* surface techniques available in the MBE chamber have allowed measuring the presence of an interface Ga-Mn-Al-As compound which, as proven by SQUID measurements, is responsible of the soft magnetic signal recorded in the ultra thin films under study.

[1] R. L. Stamps, S. Breitkreutz, J. Åkerman, A. V. Chumak, Y. Otani, G. E. Bauer, J.-U. Thiele, M. Bowen, S. A. Majetich, M. Kläui *et al.*, J. Phys. D: Appl. Phys. **47**(33), 333001 (2014).

[2] H. Saruyama, M. Oogane, Y. Kurimoto, H. Naganuma, and Y. Ando, Jpn. J. Appl. Phys., Part 1 **52**(6R), 063003 (2013).

[3] H. Kono, J. Phys. Soc. Jpn. **13**(12), 1444–1451 (1958).

[4] A. Koch, P. Hokkeling, M. G. v. d. Steeg, and K. De Vos, J. Appl. Phys. **31**(5), S75–S77 (1960).

[5] S. Nie, L. Zhu, J. Lu, D. Pan, H. Wang, X. Yu, J. Xiao, and J. Zhao, Appl. Phys. Lett. **102**(15), 152405 (2013).

[6] A. Chaturvedi, R. Yaqub, and I. Baker, J. Phys.: Condens. Matter **26**(6), 064201 (2014).

[7] E. Y. Huang and M. H. Kryder, J. Appl. Phys. **117**(17), 17E314 (2015).

[8] S. Zhao, T. Hozumi, P. LeClair, G. Mankey, and T. Suzuki, IEEE Trans. Magn. **51**(11), 1–4 (2015).

[9] J. Rial, M. Villanueva, E. Céspedes, N. López, J. Camarero, L. G. Marshall, L. H. Lewis, and A. Bollero, J. Phys. D: Appl. Phys. **50**(10), 105004 (2017).

[10] J. De Boeck, W. Van Roy, C. Bruynseraede, A. Van Esch, H. Bender, and G. Borghs, Microelectron. J. **27**(4-5), 383–392 (1996).

[11] W. Van Roy, H. Bender, C. Bruynseraede, J. De Boeck, and G. Borghs, J. Magn. Magn. Mater. **148**(1-2), 97–98 (1995).

[12] F. Jiménez-Villacorta, J. L. Marion, J. T. Oldham, M. Daniil, M. A. Willard, and L. H. Lewis, Metals **4**(1), 8–19 (2014).

[13] J. Wei, Z. Song, Y. Yang, S. Liu, H. Du, J. Han, D. Zhou, C. Wang, Y. Yang, A. Franz *et al.*, AIP Adv. **4**(12), 127113 (2014).

[14] E. M. Palmero, J. Rial, J. de Vicente, J. Camarero, B. Skärman, H. Vidarsson, P.-O. Larsson, and A. Bollero, Sci. Technol. Adv. Mater. **19**(1), 465–473 (2018).

[15] J. Coey, J. Phys.: Condens. Matter **26**(6), 064211 (2014).

[16] W. Van Roy, J. De Boeck, H. Bender, C. Bruynseraede, A. Van Esch, and G. Borghs, J. Appl. Phys. **78**(1), 398–404 (1995).

[17] J. Harbison, T. Sands, R. Ramesh, L. Florez, B. Wilkens, and V. Keramidas, J. Cryst. Growth **111**(1), 978–983 (1991).

[18] T. Sands, J. Harbison, M. Leadbeater, S. Allen, Jr., G. Hull, R. Ramesh, and V. Keramidas, Appl. Phys. Lett. **57**(24), 2609–2611 (1990).

[19] C. Duan, X. Qiu, B. Ma, Z. Zhang, and Q. Jin, Mater. Sci. Eng.: B **162**(3), 185–188 (2009).

[20] Q. Zeng, I. Baker, J. Cui, and Z. Yan, J. Magn. Magn. Mater. **308**(2), 214–226 (2007).

[21] G. A. Prinz, Science **250**(4984), 1092–1098 (1990).

[22] Z. Li-Jun, N. Shuai-Hua, and Z. Jian-Hua, Chin. Phys. B **22**(11), 118505 (2013).

[23] L. Luo, N. Anuniwat, N. Dao, Y. Cui, S. A. Wolf, and J. Lu, J. Appl. Phys. **119**(10), 103902 (2016).

[24] M. Hosoda, M. Oogane, M. Kubota, T. Kubota, H. Saruyama, S. Iihama, H. Naganuma, and Y. Ando, J. Appl. Phys. **111**(7), 07A324 (2012).

[25] A. Sakuma, J. Phys. Soc. Jpn. **63**(4), 1422–1428 (1994).